2.A.1:
2.G

Nuclear Physics **A186** (1972) 273—296; © *North-Holland Publishing Co., Amsterdam*

MULTIPLET STRUCTURE OF ^{210}Bi FROM THE ^{209}Bi(d, p) AND ^{209}Bi(α, ^{3}He) REACTIONS

C. K. CLINE, W. P. ALFORD and H. E. GOVE
Nuclear Structure Research Laboratory,
University of Rochester, Rochester, New York 14627 †
R. TICKLE
Cyclotron Laboratory,
University of Michigan, Ann Arbor, Michigan †

Received 30 December 1971

Abstract: Levels in ^{210}Bi have been studied by the ^{209}Bi(d, p)^{210}Bi reaction at 19 MeV and the ^{209}Bi(α, ^{3}He)^{210}Bi reaction at 58 MeV. Transfer l-values have been determined and spectroscopic strengths deduced by comparison with measurements of the ^{208}Pd(d, p)^{209}Pb reaction. The observed levels can be interpreted as members of multiplets arising from the weak coupling of an $h_{\frac{9}{2}}$ proton with a neutron in one of the orbits $g_{\frac{9}{2}}$, $i_{\frac{11}{2}}$, $j_{\frac{15}{2}}$, $d_{\frac{5}{2}}$, $s_{\frac{1}{2}}$, $d_{\frac{3}{2}}$ or $g_{\frac{7}{2}}$. The lowest three multiplets are quite pure, while appreciable mixing is found between members of the $\pi h_{\frac{9}{2}}\nu d_{\frac{5}{2}}$ and $\pi h_{\frac{9}{2}}\nu s_{\frac{1}{2}}$ multiplets and between members of the $\pi h_{\frac{9}{2}}\nu g_{\frac{7}{2}}$ and $\pi h_{\frac{9}{2}}\nu d_{\frac{3}{2}}$ configurations. The results show good agreement with recent theoretical calculations of the structure of ^{210}Bi.

E NUCLEAR REACTIONS ^{209}Bi(d, p), $E = 19$ MeV; measured $\sigma(E_p; \theta)$. ^{209}Bi(α, ^{3}He), $E = 58$ MeV; measured $\sigma(E_{^3\mathrm{He}}; 30°)$. ^{210}Bi deduced levels, l_n, J, π, S. Natural target.

1. Introduction

The low-lying states in ^{210}Bi are expected to consist of a number of multiplets arising from the coupling of a neutron and a proton, each in one of the single-particle states outside the ^{208}Pb core. The proton single-particle states have been studied in the ^{208}Pb(^{3}He, d) reaction [1, 2]) while the neutron states have been investigated in the ^{208}Pb(d, p) reaction [3, 4]) and the ^{208}Pb(t, d) reaction [5]). Both sets of orbitals are thus fairly well known. The energies of these orbitals in their respective single-particle nuclei and the unperturbed centroid energies of the low-lying particle-particle multiplets in ^{210}Bi are shown in fig. 1. For each multiplet, the range of spin values is also indicated.

Much of the experimental information on ^{210}Bi has come from the ^{209}Bi(d, p) reaction. This reaction is expected to populate states in ^{210}Bi arising from the coupling of the $h_{\frac{9}{2}}$ proton in the ^{209}Bi ground state with a neutron in one of the available single-particle states. The corresponding multiplets are shown as heavy lines in fig. 1. The work of Mukherjee and Cohen [3]) and of Erskine, Buechner and Enge [6]) demonstrates that many of the levels in ^{210}Bi appear in clusters. Evidence

† Work supported by a grant from the National Science Foundation.

that these clusters correspond to the weak coupling proton-neutron multiplets shown in fig. 1 is contained in the angular distributions from the work of Erskine *et al.* [6]) and Mukherjee [7]). Erskine also presents tentative spin assignments for members of the ground state multiplet which are based on the assumption that the strengths of the transitions should be proportional to $(2J+1)$. His spin assignments agree well with theoretical predictions. Other experimental evidence on ^{210}Bi has come from

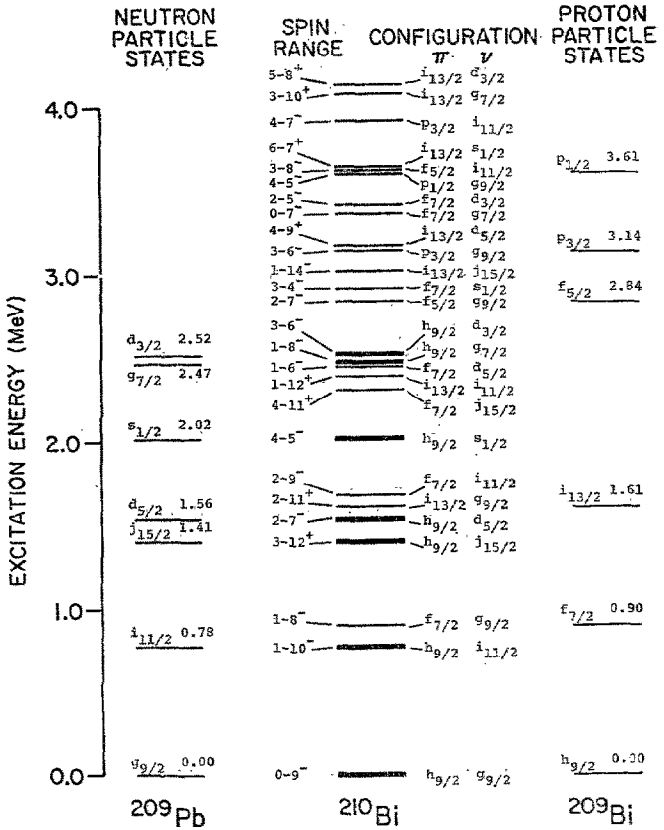

Fig. 1. Summary of the single-particle states in ^{209}Pb and ^{209}Bi and of the simple weak-coupling particle-particle configurations in ^{210}Bi. The configurations indicated by heavy broad lines are those which should be populated in neutron transfer reactions on a ^{209}Bi target.

the (d, pγ) reaction [8, 9]) and the (n, γ) reaction [10]) on ^{209}Bi. These reactions have provided spin values, excitation energies and, occasionally, lifetime measurements for a number of levels.

Theoretical calculations [11–13]) of the structure of ^{210}Bi indicate that many of the low-lying levels should arise from the relatively pure proton-neutron configurations shown in fig. 1. However, for some levels, significant mixing of two or more configurations is predicted. For example, in Kuo's calculations [13]) the 1^-, 2^-, 3^- and 5^-

states of the $\pi h_{\frac{9}{2}} \nu i_{\frac{13}{2}}$ and $\pi f_{\frac{7}{2}} \nu g_{\frac{9}{2}}$ multiplets are predicted to be mixed as are the 3^-, 4^-, 5^- and 6^- states of the $\pi h_{\frac{9}{2}} \nu g_{\frac{7}{2}}$ and $\pi h_{\frac{9}{2}} \nu d_{\frac{3}{2}}$ multiplets.

The purpose of the present work was to repeat the ^{209}Bi(d, p) reaction with sufficient bombarding energy and proton energy resolution to permit the determination of transfer *l*-values for all observed levels. In this way, it was hoped that the levels corresponding to the members of the seven anticipated multiplets could be clearly identified. It should also be possible to determine the extent of configuration mixing for comparison with theoretical predictions.

Earlier studies [4]) of the ^{208}Pb(d, p)^{209}Pb reaction have shown that the detailed shapes of the experimental angular distributions are fitted only moderately well by conventional DWBA calculations. This result has the consequence that mixtures of different *l*-values in transitions observed in the ^{209}Bi(d, p)^{210}Bi reaction could not be reliably extracted by comparison with DW calculations. In order to obtain such information, it appeared necessary to have careful measurements of the ^{208}Pb(d, p)^{209}Pb angular distributions at the same deuteron energy (19 MeV) as the bismuth measurements. These distributions could then be used as empirical curves to which the bismuth data could be compared.

In order to aid in the interpretation of the results for the $i_{\frac{13}{2}}$ and $j_{\frac{15}{2}}$ transfers which are weakly excited in the (d, p) reaction, measurements were also made on the ^{209}Bi(α, ^{3}He)^{210}Bi reaction which populates these transitions strongly.

2. Experimental

2.1. THE (d, p) REACTIONS

The measurements of the (d, p) reaction were carried out using a 19.0 MeV beam from the University of Rochester Tandem Van de Graaff accelerator. The ^{209}Bi target consisted of a 1 mm wide vertical line of bismuth metal evaporated to a thickness of about 90 μg/cm^2 onto a 20 μg/cm^2 carbon backing. A similar line target was prepared for studying the ^{208}Pb(d, p) reaction by evaporating metallic lead enriched to 99.47 % in the mass 208 isotope onto a carbon backing. The thickness of the lead target is estimated to be about 80 μg/cm^2. With the line targets, it was possible to use 3 mm wide slits at the entrance to the scattering chamber so that the amount of slit scattering of the beam could be kept to a minimum.

Proton spectra were recorded in Kodak type NTB nuclear emulsions placed in the focal plane of the Enge split-pole magnetic spectrograph. The thickness of the emulsions was 50 μm. Aluminium absorbers with a thickness of about 0.794 mm were placed in front of the plates to stop all particles focussed by the spectrograph except the protons.

For both (d, p) reactions, proton spectra were recorded at 5° intervals between 10° and 60°. Two sets of exposures were taken for the ^{208}Pb(d, p) reaction with exposure times differing by a factor of about 10. Peaks corresponding to all seven available single-neutron levels were analyzed from the short exposures. The long

exposures were used to get more reliable data on the $i_{\frac{13}{2}}$ and $j_{\frac{15}{2}}$ levels which are only weakly populated in the (d, p) reaction because of the high transfer *l*-values involved. All plates were scanned in $\frac{1}{4}$ mm steps.

A typical spectrum for the ^{209}Bi(d, p) reaction taken at 40° in the lab system is shown in fig. 2. The energy resolution for the groups from the reaction of interest is typically about 10 keV FWHM. Much broader groups from the (d, p) reaction on ^{12}C and ^{16}O are indicated in fig. 2 while at more forward angles, protons from reactions on ^{14}N were also evident. The level of the background in the various spectra was generally higher at more forward angles.

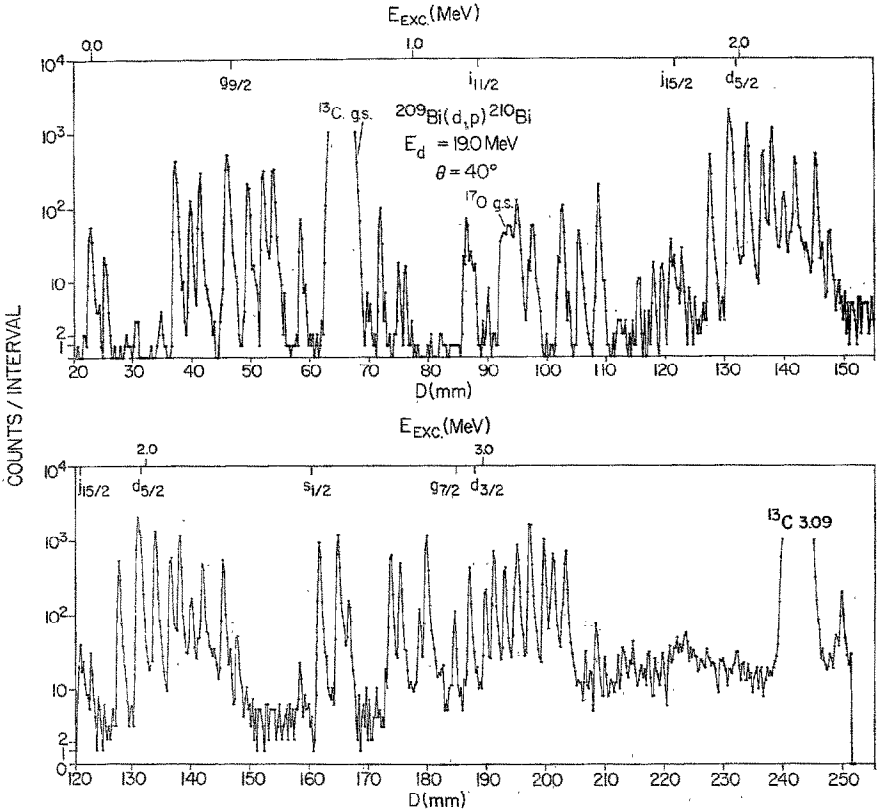

Fig. 2. Experimental proton spectrum from the ^{209}Bi(d, p) reaction at a bombarding energy of 19 MeV measured at 40° in the laboratory system. The relative positions of the single-neutron states in ^{209}Pb are indicated along the top of the figure and have been shifted so that the $g_{\frac{9}{2}}$ level corresponds to the centroid of the ground state multiplet in ^{210}Bi.

Since it was not intended to make a detailed study of ^{209}Pb, the plates for the ^{208}Pb(d, p) reaction were scanned only in the regions around the peaks corresponding to the seven single-particle levels in the product nucleus. As was the case for the

^{209}Bi(d, p) reaction, the resolution was found to be about 10 keV FWHM. The background level in the spectra increased dramatically in going to more forward angles. Once again, impurity groups from the ^{12}C(d, p) and ^{16}O(d, p) reactions were evident. The raw 40° data are shown in fig. 3.

Energies of the different reaction groups from both reactions were obtained from the plate positions using the spectrograph field strengths. The spectrograph has recently been recalibrated using 10 MeV deuterons elastically scattered from a ^{232}Th target by varying the spectrograph field settings. The results of this calibration are in

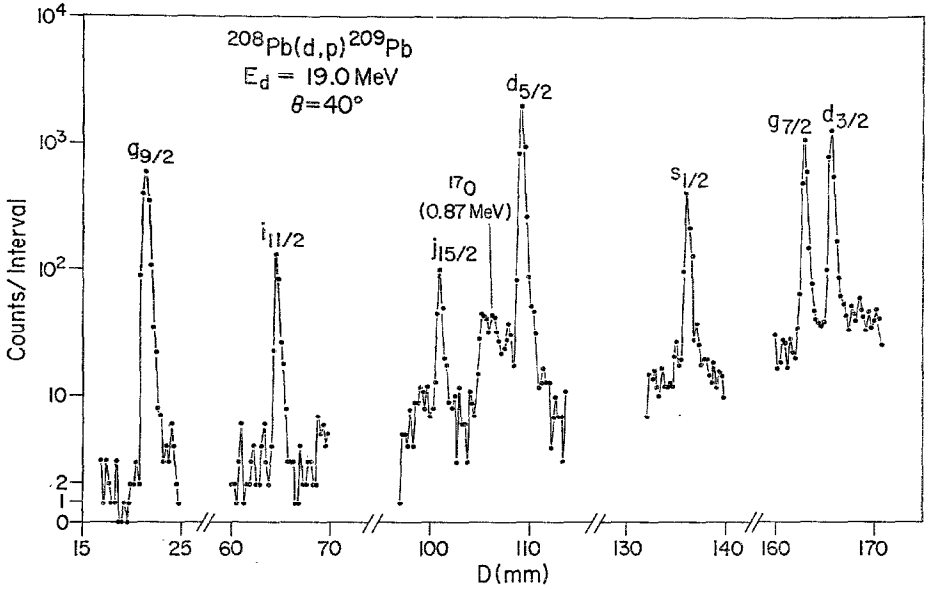

Fig. 3. Selected regions of the experimental proton spectrum from the ^{208}Pb(d, p) reaction at a bombarding energy of 19 MeV measured at 40° in the laboratory.

good agreement with a much earlier calibration carried out using a Th C′ α-source. From a comparison of these results and from comparisons of level energies measured with the spectrograph and with high-resolution Ge(Li) detectors, it is concluded that calibration errors result in an uncertainty of less than 2 keV for excitation energies measured relative to the known ground state transition. These errors should be less than those resulting from emulsion shifts during developing and evidenced in the scatter of energy values found from exposures at different angles.

In order to obtain absolute cross sections for the population of the levels seen in this work, and to normalize all the data for a given reaction taken at many different angles, the deuterons elastically scattered from the target were monitored during each plate exposure. This was accomplished using a NaI detector mounted at an angle of 45°. The elastic scattering cross sections used to obtain an absolute normalization were obtained from DWBA calculations described later.

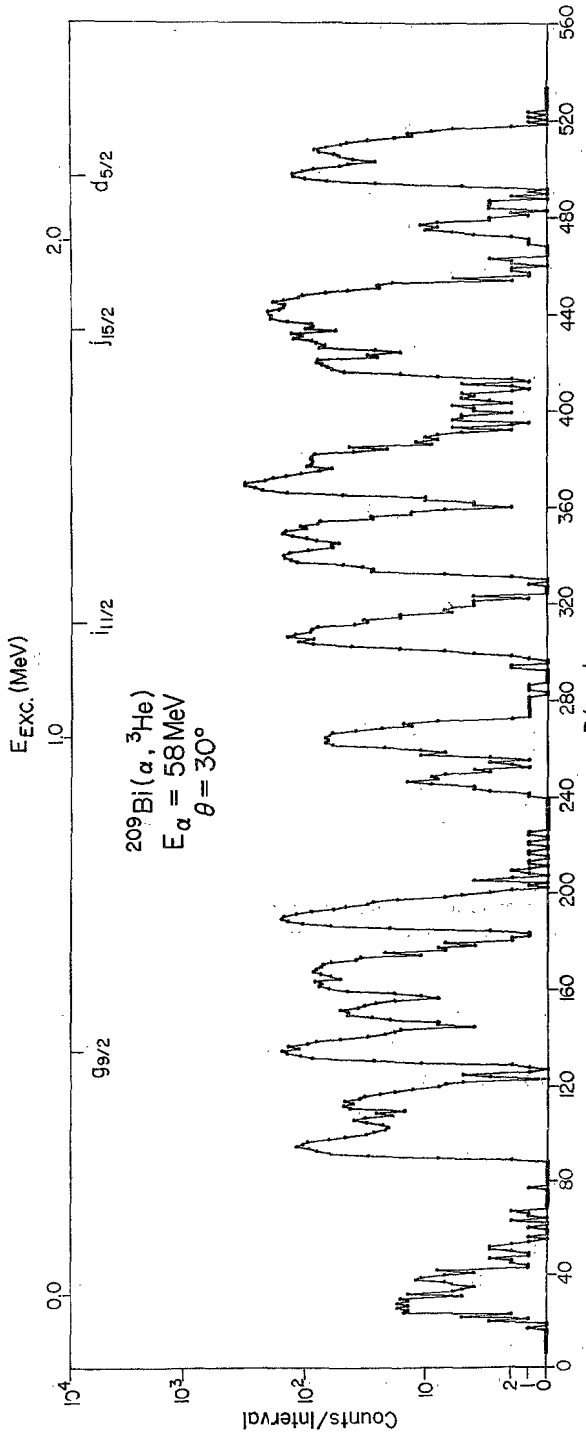

Fig. 4. Experimental ^{3}He spectrum from the ^{209}Bi(α, ^{3}He) reaction at a bombarding energy of 58 MeV measured at 30° in the laboratory. The single-neutron states are indicated as in fig. 2.

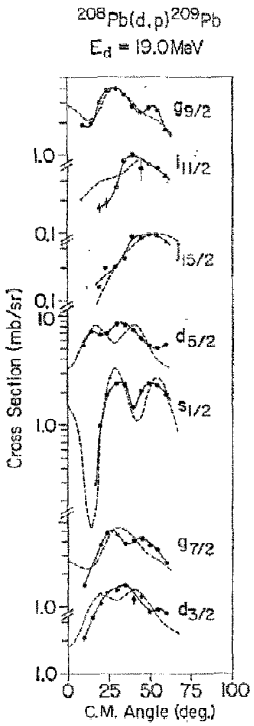

Fig. 5. Proton angular distributions from the ^{208}Pb(d, p) reaction at 19 MeV. The points represent the data. The dashed curves are the results of DWBA calculations. The solid curves have been drawn through the points and have been used in the analysis of the ^{209}Bi(d, p) angular distributions.

TABLE 1

Summary of optical model potentials [a])

	V_0 (MeV)	r_0 (fm)	a (fm)	W_0 (MeV)	W_d (MeV)	r'_0 (fm)	a' (fm)	r_c (fm)	λ	β [b]) (fm)	R [c]) (fm)
p	52	1.25	0.65	0	7.5	1.25	0.76	1.25		0.85	
d	100	1.14	0.89	0	13.9	1.33	0.75	1.30		0.54	1.25
bound n	[d])	1.20	0.65						25		

[a]) Optical potential:

$$U(r) = -U_C(r) - V_0(1+e^x)^{-1} - iW_0(1+e^{x'})^{-1} + 4iW_d \frac{d}{dx'}(1+e^{x'})^{-1}.$$

Bound state:

$$U_n(r) = -V_0\left[1 - \frac{\lambda}{ra}\left(\frac{\hbar}{2m_pc}\right)^2 \sigma \cdot l \frac{d}{dx}\right](1+e^x)^{-1},$$

$$x = (r - r_0 A^{\frac{1}{3}}),$$

$U_C(r)$ is the Coulomb potential for a uniformly charged sphere of radius $R_c = r_c A^{\frac{1}{3}}$.

[b]) Non-locality range.

[c]) Range of n-p interaction.

[d]) Adjusted to reproduce the neutron binding energy.

2.2. THE (α, ^{3}He) DATA

The ^{209}Bi(α, ^{3}He) reaction was studied using a 58 MeV α-particle beam from the University of Michigan 83" sector focussed cyclotron. The target was made of self-supporting bismuth metal and had a thickness of 150 μg/cm^2. Two ^{3}He ion energy spectra were measured at an angle of 30° in the laboratory; one using a single 180° magnetic spectrometer and the other using two such magnets. In each case the momentum analyzed ^{3}He ions were recorded in 100 μm thick Ilford K-0 emulsions placed at the image surface. Aluminium absorbers with a thickness of 0.35 mm were placed in front of the plates to absorb scattered particles and to enhance the ^{3}He track density in the emulsions. The plates were scanned in ½ mm wide strips at 1 mm intervals. The results obtained with the double spectrograph are shown in fig. 4. This spectrum extends up to about 2.2 MeV of excitation and no strong states were evident above this energy.

The energy resolution of the double-magnet data is about 26 keV FWHM, while for the single-magnet data it is 47 keV FWHM. Because of this relatively poor energy resolution, no attempt was made to use this spectrum to identify and determine the energies of reaction groups. This was only done for two levels which were seen in the (α, ^{3}He) but not in the (d, p) data. An energy calibration for the (α, ^{3}He) spectrum was obtained using the plate positions of a few of the stronger and better resolved levels together with the energies of these levels as determined in the (d, p) work. In addition, no attempt was made to determine absolute cross sections for the α-particle induced reactions. The double-magnet data were corrected for variations in the solid angle across the spectrum by comparing the intensities of cluster of levels from the single- and double-magnet data. The corrected data could then be used to determine the relative intensities of the individual levels within the clusters.

3. Results and analysis for ^{209}Pb

Angular distributions of protons populating the seven single-particle states in ^{209}Pb are shown in fig. 5. The error bars on the present data points represent the uncertainties due to counting statistics and background subtraction.

The data in fig. 5 are compared with DWBA calculations using the code DWUCK [14]). The optical-model parameters used in the analysis are those used by Muehllehner *et al.* [4]) in an earlier study of this reaction. The parameters are given in table 1. Calculations include a finite-range interaction and non-locality corrections in the incident and outgoing scattered waves. No radial cut-off was used in the calculations.

It is seen from fig. 5 that the DWBA calculations provide only fair agreement with the data. While such calculations may be adequate to identify unique l-transfers involved in stripping on a target with zero spin, it would be difficult to determine the relative contributions from transitions with different l-values, which can arise in the ^{209}Bi(d, p)^{210}Bi measurements.

Spectroscopic factors obtained from the analysis of the ^{208}Pb(d, p)^{209}Pb results are shown in table 2. The agreement with earlier measurements [4, 5, 15]) is quite satisfactory.

TABLE 2

Summary of experimental results on ^{209}Pb

	Excitation energies (MeV)					Spectroscopic factors					
	(d, p)			(t, d)	present	(d, p) ref. [4])			(t, d)	(p, p_0)	present
l_j	ref. [3])	ref. [22])	ref. [4])	ref. [5])	work	15 MeV	20 MeV	25 MeV	ref. [5])	ref. [15])	work
$g_{\frac{9}{2}}$	0	0	0	0	0	0.87	0.77	0.67	0.93	0.97	0.85
$i_{\frac{11}{2}}$	0.77	0.774	0.79	0.781±5	0.774±3	1.17	0.78	0.94	1.05		1.14
$j_{\frac{15}{2}}$	1.41		1.42	1.428	1.419±2	0.96	0.79	1.13	0.51		0.74
$d_{\frac{5}{2}}$	1.56	1.563	1.56	1.573	1.561±3	0.83	1.05	1.00	0.86	0.85	0.86
$s_{\frac{1}{2}}$	2.03	2.015	2.01	2.039	2.028±2	0.80	0.90	0.93	0.86	0.90	0.90
$g_{\frac{7}{2}}$	2.47	2.483	2.47	2.496	2.489±3	1.08	1.08	1.17	0.90	0.84	1.04
$d_{\frac{3}{2}}$	2.51	2.527	2.51	2.542	2.533±3	0.88	1.07	1.17	0.83	0.86	0.96

4. Results and analysis for ^{210}Bi

Over 60 levels in ^{210}Bi have been seen in this work with over 50 of them having energies below 3.3 MeV. The levels seen include all those previously reported in the literature, plus a number of new ones. In addition, preliminary (d, p) results of Kolata and Daehnick [16]) include several weak levels not seen here. The measured excitation energies found in this and earlier work are summarized in table 3. The energy values for ^{210}Bi have quoted uncertainties which represent the average magnitude of the deviation of several determinations from the mean energy. In general, the present energy values agree quite well with those found in other experiments.

From fig. 2 it can be seen that the strongly populated levels in ^{210}Bi form clusters corresponding to the expected multiplets. The relative positions of the corresponding single neutron states in ^{209}Pb are indicated in the figure with the $g_{\frac{9}{2}}$ ground state placed so as to coincide with the centroid of the ground state multiplet in ^{210}Bi.

Beyond an excitation energy of 3.3 MeV a more or less continuous background of protons is observed with only a few weakly excited levels superposed up to an energy of about 4 MeV. In preliminary runs, a search was made up to 7 MeV of excitation, but no distinct groups were observed beyond 4 MeV.

The angular distributions for many of the strong transitions observed in this work are shown in figs. 6 through 12. The error bars in these figures are estimates of the statistical uncertainties associated with the number of tracks in the peaks and the level of the background.

The usual procedure for obtaining transfer l-values and spectroscopic strengths is to compare such data with DWBA calculations. As noted above, DWBA calcula-

TABLE 3

Summary of excitation energies for ^{210}Bi

Level no.	Present work	Erskine [6]) *et al.*	Kolata [16]) and Daehnick	Ellegaarde [9]) *et al.*	Ley [8])	Motz [10]) *et al.*
1	0	0	0	0	0	0
2	46±3	47	47	47	47	47
3	270±2	268	272	271	268	271
4	317±2	320	320	320	319	320
5	346±2	347	347	348	349	348
6	434±2	433	436	{433, 439}	430	{433, 439}
7	501±2	501	502	503	504	502
8	549±2	547	549	549	546	550
9	580±2	581	582	582	578	582
10	665±2	672	668		665	673
11	912±2	912	915		912	916
12	966±2		971			972
13	991±3		993			994
14	1178±2	1172	1181		1181	(1196)
			(1194)			
15	1202±3		1205			1208
16	1243±2		1247			
17	1315±6	1325	{1317, 1336}		1325	1336
18	1334±3					
19	1373±2	1372			1372	
20	1384±2		1382			
21	1458±5	1460				
22	1470±3		1473		1473	
23	1522±3	1517	1525		1517	
24	1582±2	1577	1583		1586	
25	1701±2		1705			
26	1746±1		1750			
27	1771±4		1775			
28	1799±3		1801			
			1812			
29	1831±4		1835		(1910)	
30	1919±2	1916	1922		1925	
31	1975±3	1972	1981		{1962, 1978}	
32	1984±3					
33	2029±3	2027	2033		2030	
34	2072±10					
35	2076±3	2075	2080		2081	
36	2103±3	2102	2107		{2100, 2105}	
37	2110±10					
38	2133±3	2138	2143		2138	
39	2173±3	2173	2176		2178	
40	2234±3	2235	2236		2234	
41	2276±4		2280			
			2314			
			(2340)			
42	2460±3		2464			

TABLE 3 (continued)

Level no.	Present work	Erskine [6]) *et al.*	Kolata [16]) and Daehnick	Ellegaarde [9]) *et al.*	Ley [8])	Motz [10]) *et al.*
43	2520±3	2517	2523		{2516 2525	
44	2575±3	2572	2578		2576	
45	2606±4	2607	2611		2606	
46	2729±4	2727	2734		2731	
47	2759±4	2756	2762		{2756 2764	
48	2816±4		2819			
49	2835±4	2833	2839		2835	
50	2915±4	2915	2920		2915	
51	2961±3	2960	2964		2962	
52	3006±3	3007	3011		3007	
53	3031±3	3033	3035		3027	
54	3063±3	3064	3067		3067	
55	3098±4	3095	3102		3100	
56	3136±4	3135	3138		3134	
57	3177±3	3175	3180		3178	
58	3202±3	3205	3206		3206	
59	3234±3		3242			
60	3293±2		3299			
61	3324±3		3330			
62	3399±4					
63	3435±10					
64	3472±4					
65	4005±3					
66	4021±3					

tions for the ^{208}Pb(d, p)^{209}Pb reaction at 19 MeV provide only fair fits to the experimental data. For this reason, we have chosen to use the measured cross sections for the transitions to the low-lying single-particle states in ^{209}Pb in place of the DWBA calculations for the analysis of the present data. This procedure rests on the assumption that the intrinsic cross sections are similar in angular variation and magnitude for the (d, p) reactions on ^{208}Pb and ^{209}Bi. This assumption is supported by the results of DWBA calculations, and by the actual data comparisons discussed below.

With the assumption that $\sigma_{DW}(^{208}\text{Pb}) = \sigma_{DW}(^{209}\text{Bi})$, the spectroscopic strength for a level of spin J excited by transfer of a particle with given (l, j) is given by

$$G_J(l,j) = \frac{2J+1}{2I+1} C^2S(^{210}\text{Bi}) = \frac{d\sigma/d\Omega(^{210}\text{Bi})}{d\sigma/d\Omega(^{209}\text{Pb})} (2j+1) C^2S(^{209}\text{Pb}).$$

Here $I = \frac{9}{2}$ is the spin of the ^{209}Bi target. The cross section and spectroscopic factor for the ^{209}Pb refer, of course, to the single-particle state of given (l, j). Thus the strengths in ^{210}Bi are being determined relative to the strengths in ^{209}Pb. We note from table 2 that the measured spectroscopic factors in ^{209}Pb are all close to unity, and we have assumed that the states are, in fact, single-particle states with $S = 1$.

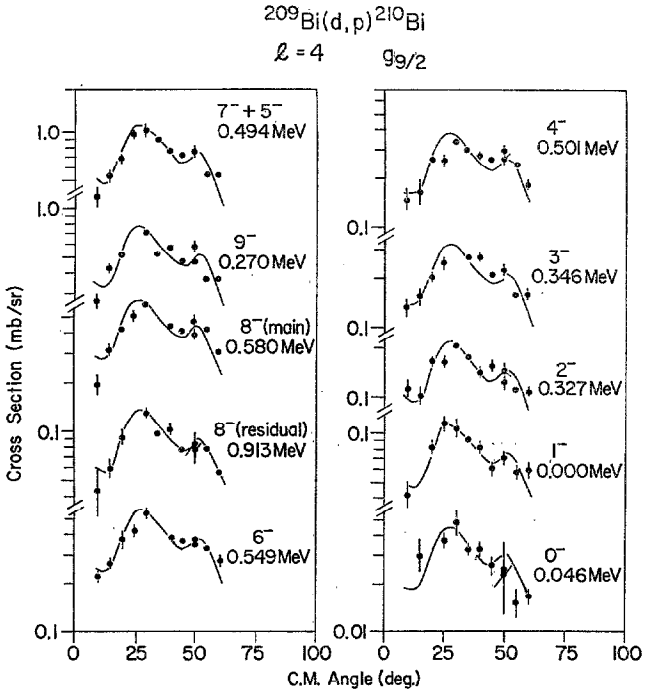

Fig. 6. Angular distributions for transitions assigned as $g_{\frac{9}{2}}$ neutron transfers. The points show the data, and the solid curves are the fits to the data with the corresponding ^{208}Pb(d, p) experimental angular distribution.

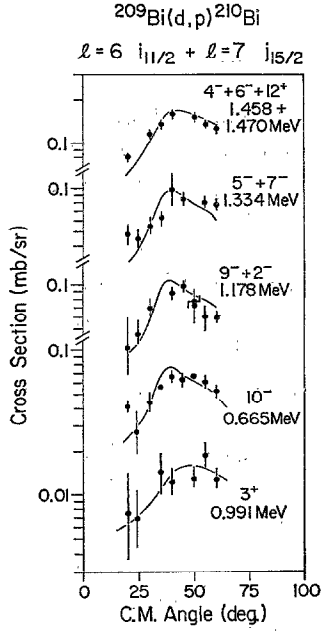

Fig. 7. Angular distributions for transitions assigned as $i_{\frac{11}{2}}$ or $j_{\frac{15}{2}}$ neutron transfers. The points and curves have the same significance as in fig. 6.

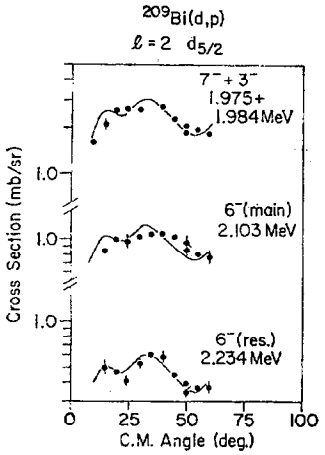

Fig. 8. Angular distributions for transitions assigned as pure $d_{\frac{5}{2}}$ neutron transfers. The points and curves have the same significance as in fig. 6.

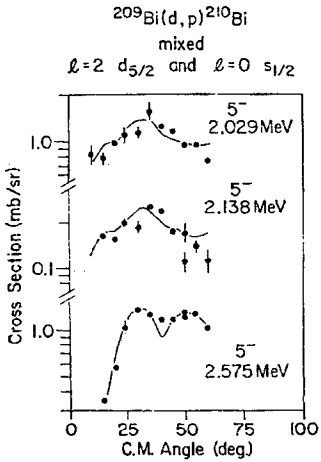

Fig. 9. Angular distributions for transitions assigned as mixed $d_{\frac{5}{2}}$ and $s_{\frac{1}{2}}$ neutron transfer. The points show the data while the solid curves are the fits obtained using the experimental ^{208}Pb (d, p) angular distributions in a mixed-l analysis.

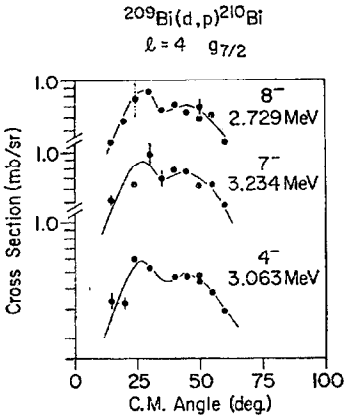

Fig. 10. Angular distributions for transitions assigned as $g_{\frac{7}{2}}$ neutron transfers. The points and curves have the same significance as in fig. 6.

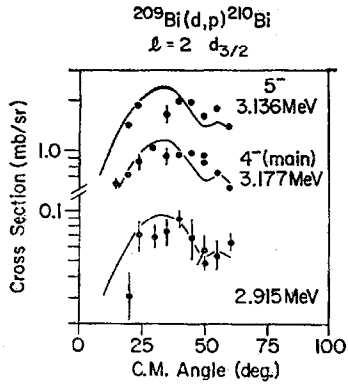

Fig. 11. Angular distributions for transitions assigned as $d_{\frac{3}{2}}$ neutron transfers. The points and curves have the same significance as in fig. 6.

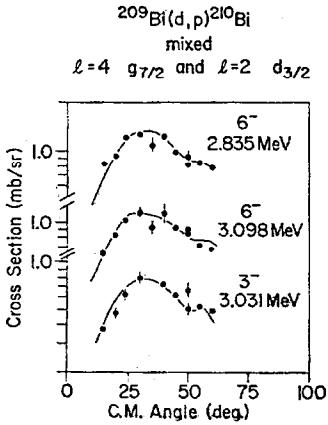

Fig. 12. Angular distributions for transitions assigned as mixed $g_{\frac{7}{2}}$ and $d_{\frac{3}{2}}$ neutron transfers. The points and curves have the same significance as in fig. 9.

TABLE 4
Summary of spectroscopic strengths for ^{210}Bi

Level	Energy (keV)	Transfer l	Orbital	(d, p) G	(α, ^{3}He) G	J^π	Allowed J^π [b]
1	0	4	$g_{\frac{9}{2}}$	0.29		1^-	
2	46	4	$g_{\frac{9}{2}}$	0.11		0^-	
3	270	4	$g_{\frac{9}{2}}$	1.95		9^-	
4	317	4	$g_{\frac{9}{2}}$	0.54		2^-	
5	346	4	$g_{\frac{9}{2}}$	0.81		3^-	
6	434	4	$g_{\frac{9}{2}}$	2.7		$5^-, 7^-$	
7	501	4	$g_{\frac{9}{2}}$	1.06		4^-	
8	549	4	$g_{\frac{9}{2}}$	1.34		6^-	
9	580	4	$g_{\frac{9}{2}}$	1.49		8^-	
10	665	6	$i_{\frac{13}{2}}$	1.84	2.1 [a]	10^-	7–11
11	912	4	$g_{\frac{9}{2}}$	0.31		8^-	7–9
12	966	(6)	$(i_{\frac{13}{2}})$	0.36		1^-	1–3
13	991	7	$j_{\frac{15}{2}}$	0.78	0.7 [a]	3^+	2–4
14	1178	6	$i_{\frac{13}{2}}$	2.5	2.8	$(9^-, 2^-)$	6–10
15	1202	(6)	$(i_{\frac{13}{2}})$	0.70		3	3–5
16	1243						
17	1315						
18	1334	6	$i_{\frac{13}{2}}$	2.3	3.25	$5^-, 7^-$	4–6
19	1373	(6)	$(i_{\frac{13}{2}})$	2.9	2.9	$(8^-, 3^-)$	
20	1383						
21	1458	6	$i_{\frac{13}{2}}$	2.5	2.5	(4^-)	
22	1470	6	$i_{\frac{13}{2}}$			6^-	
		7	$j_{\frac{15}{2}}$	3.3	2.6	12^+	
23	1522	7	$j_{\frac{15}{2}}$	3.05	1.2	(4^+)	1–4
24	1582	2	$d_{\frac{5}{2}}$	0.12		2^-	
25	1701	7	$j_{\frac{15}{2}}$	0.86	1.15	5^+	
26	1746	7	$j_{\frac{15}{2}}$	0.97	2.36	10^+	
27	1771	(7)	$(j_{\frac{15}{2}})$	1.31	1.37	6^+	
28	1799	7	$j_{\frac{15}{2}}$	2.2	3.0	$8^+, 11^+$	
29	1831	(7)	$(j_{\frac{15}{2}})$	2.4	1.6	7^+	
30	1919	2	$d_{\frac{5}{2}}$	0.32		2^-	0–3
31	1975	2	$d_{\frac{5}{2}}$	2.1		7^-	7,8
32	1984					3^-	
33	2029	2	$d_{\frac{5}{2}}$	0.76 ± 0.16		5^-	4–8
		0	$s_{\frac{1}{2}}$	0.24 ± 0.17			
34	2072	7	$j_{\frac{15}{2}}$		2.3	9^+	
35	2076	2	$d_{\frac{5}{2}}$	0.45		4^-	0–4
36	2103	2	$d_{\frac{5}{2}}$	0.82		6^-	6–8
37	2110	7	$j_{\frac{15}{2}}$		1.37	(11^+)	
38	2138	2	$d_{\frac{5}{2}}$	0.14 ± 0.03		5^-	
		0	$s_{\frac{1}{2}}$	0.04 ± 0.04			
39	2173	2	$d_{\frac{5}{2}}$	0.29 ± 0.05		4^-	2–5
		0	$s_{\frac{1}{2}}$	0.06 ± 0.06			
40	2234	2	$d_{\frac{5}{2}}$	0.41		6^-	5–7
41	2276	2	$d_{\frac{5}{2}}$	0.042			
42	2400						
43	2520	0	$s_{\frac{1}{2}}$	0.71 ± 0.06		4^-	3,4
		2	$d_{\frac{5}{2}}$	0.08 ± 0.05			

TABLE 4 (continued)

Level	Energy (keV)	Transfer	Orbital	(d, p) G	(α, ^{3}He) G	J^π	Allowed J^π [b]
44	2575	0 2	$s_{\frac{1}{2}}$ $d_{\frac{5}{2}}$	0.90±0.08 0.20±0.06		5$^-$	3–9
45	2606	0 2	$s_{\frac{1}{2}}$ $d_{\frac{5}{2}}$	0.13±0.04 0.037±0.026		(4$^-$)	3–9
46	2729	4	$g_{\frac{7}{2}}$	1.32		8$^-$	7–11
47	2759	4 2	$g_{\frac{7}{2}}$ $d_{\frac{3}{2}}$	0.46±0.24 0.16±0.09		3$^-$	1–6
48	2816	4	$g_{\frac{7}{2}}$	0.23		1$^-$	
49	2835	2 4	$d_{\frac{3}{2}}$ $g_{\frac{7}{2}}$	0.64±0.12 0.53±0.38		(6$^-$)	4–8
50	2915	2	$d_{\frac{3}{2}}$	0.063			
51	2961	4 2	$g_{\frac{7}{2}}$ $d_{\frac{3}{2}}$	0.32±0.21 0.15±0.08		4$^-$	4–8
52	3006	4	$g_{\frac{7}{2}}$	0.45		2$^-$	0–4
53	3031	4 2	$g_{\frac{7}{2}}$ $d_{\frac{3}{2}}$	0.40±0.35 0.34±0.14		(3$^-$)	3–6
54	3063	4	$g_{\frac{7}{2}}$	0.90		4$^-$	4$^-$
55	3098	4 2	$g_{\frac{7}{2}}$ $d_{\frac{3}{2}}$	0.96±0.39 0.37±0.16		6$^-$	6$^-$
56	3136	(2)	($d_{\frac{3}{2}}$)	1.44		5$^-$	5–7
57	3177	(2)	($d_{\frac{3}{2}}$)	0.69		(4$^-$)	2–4
58	3202	4	$g_{\frac{7}{2}}$	1.27		(5$^-$)	2–5
59	3234	4	$g_{\frac{7}{2}}$	1.41		7$^-$	

[a]) The (α, ^{3}He) strengths have been normalized to these theoretical values for these two levels (see text).

[b]) These values have been summarized from refs. [8–10]).

Transfer l-values for many levels have been determined using as standard shapes the smooth curves drawn through the experimental points of the ^{208}Pb(d, p)^{209}Pb angular distributions shown in fig. 5. The fits of these standard curves to the Bi data are shown in figs. 6–12. For many levels it is seen that the measured angular distributions on ^{209}Bi are fitted very well by the empirical curves from ^{208}Pb, as expected from the results of DWBA calculations. Such calculations further predict that the shapes of the angular distributions are not affected by changes of a few hundred keV in reaction Q-value. For the $i_{\frac{11}{2}}$, $d_{\frac{5}{2}}$ and $s_{\frac{1}{2}}$ neutron transfers, the Q-dependence of the cross sections would entail corrections to the data of less than 7 %, and these effects have been neglected because of the other uncertainties in the data. For the $g_{\frac{9}{2}}$ and $j_{\frac{15}{2}}$ neutron transfer where the corrections for individual levels were as large as 11 % and 25 % respectively, the Q-value dependence of the cross section was taken into account in arriving at spectroscopic strengths. Finally, because of the uncertainties in the strengths obtained from the mixed-l analyses for $g_{\frac{7}{2}}$ and $d_{\frac{3}{2}}$ transfer, no Q-dependence correction was made on these data.

It may be noted that the (d, p) angular distributions do not allow a clear discrimination of $l = 6$ from $l = 7$ transitions. Assignments for levels populated with these

angular momentum transfers have been facilitated by a comparison between the (d, p) and (α, ^{3}He) results, since the latter reaction strongly favours high-l transfers [17]). The l-values have been obtained from the (α, ^{3}He) intensities by assuming, on the basis of the (d, p) results, that the 665 keV level is the 10^- member of the $\pi h_{\frac{9}{2}} \nu i_{\frac{13}{2}}$ multiplet and that the 991 keV level is the 3^+ member of the $\pi h_{\frac{9}{2}} \nu j_{\frac{15}{2}}$ multiplet. These have been assigned their theoretical single-particle spectroscopic strengths of 2.1 and 0.7 respectively. Comparison of possible $l = 6$ and $l = 7$ spectroscopic strengths for the other levels with the corresponding approximate values from the (d, p) reaction gives an indication of the transfer l. The $j_{\frac{15}{2}}$ transfer is favored over the $i_{\frac{13}{2}}$ in the (α, ^{3}He) reaction while the situation is reversed in the (d, p) case. The Q-dependence of the (α, ^{3}He) cross sections has been estimated from DWBA calculations using the parameters suggested by Alford and Burke [18]). It amounts to about a 15 % decrease in the cross section from the lowest to highest-energy members of the multiplets, and this correction has been applied to the data.

For some higher-energy states, the (d, p) data could not be reasonably well fitted with one of the standard shapes, and an analysis was carried out assuming a mixture of two l-values contributing to the transition.

A summary of the transfer l-values and strengths determined in this experiment is given in table 4. The proposed transfer orbitals were taken to be those of the corresponding single-neutron level in ^{209}Pb. The spin assignments given in the table have been arrived at from a number of considerations and in many cases are not unique. Primarily because of the apparent success of the weak-coupling model in describing the ground state multiplet [9]), spin values have been assigned so as to be consistent with a $(2J+1)$ cross section weighting for levels in a single weak-coupling multiplet. The present assignments, which are shown in table 4, are also consistent with the spin values allowed by γ-ray studies [8-10]). These allowed spin values are also shown in the table. States of unusually high intensity were generally either known or assumed to be unresolved doublets. In cases where ambiguities exist in the data, the level orderings for a given (l, j) transfer predicted by theoretical calculations have been used in making the tentative spin assignments shown in table 4. The identification of various states as members of weak-coupling multiplets may be discussed with reference to this table.

4.1. THE $g_{\frac{9}{2}}$ NEUTRON TRANSFERS

The angular distributions of transitions to the low-lying states of ^{210}Bi are seen from fig. 6 to be well fitted by the $l = 4$, $g_{\frac{9}{2}}$ standard curve. The spins of all levels up to 580 keV have been independently determined [9]) by assuming that the ten lowest levels would have one level each of spin 0^- to 9^- as predicted for the ground state weak-coupling multiplet. These spin assignments are shown in table 4, and the measured strengths are found to be proportional to $(2J+1)$ within the experimental uncertainties. The possible exception to this is the 8^- level at 580 keV. However the $l = 4$ level at 912 keV is also assigned a spin of 8 [ref. [10])], and the total strength of the

two 8^- states is proportional to $(2J+1)$. Thus the present data are consistent with a description of the low-lying states populated by $l = 4$ transfer as members of a simple weak-coupling multiplet, with some configuration mixing in the 8^- state.

4.2. THE $i_{\frac{13}{2}}$ AND $j_{\frac{15}{2}}$ NEUTRON TRANSFERS

States from the $\pi h_{\frac{9}{2}} \nu i_{\frac{13}{2}}$ and $\pi h_{\frac{9}{2}} \nu j_{\frac{15}{2}}$ multiplets are only weakly populated in the ^{209}Bi(d, p) reaction because of the high transfer l-values involved. Analysis of these two multiplets has therefore relied rather heavily on the ^{209}Bi(α, ^{3}He) data. As has already been indicated, the energies of the levels have generally been obtained from the (d, p) data because of its better resolution while the (α, ^{3}He) data have been used to differentiate $l = 6$ and $l = 7$ transitions from each other and from weak fragments of states populated by low-l transfer as well as to obtain the relative intensities of the levels.

Angular distributions from the (d, p) reaction for a few of the stronger and more cleanly resolved levels in the $\pi h_{\frac{9}{2}} \nu i_{\frac{13}{2}}$ and $\pi h_{\frac{9}{2}} \nu j_{\frac{15}{2}}$ multiplets are shown in fig. 7. Angular distributions for other levels in these configurations were generally too fragmentary to provide good l-determinations, and the (d, p) data have been used mainly to determine excitation energies.

Comparison of the (α, ^{3}He) and (d, p) results indicates that levels such as 16 and 17 which are seen only weakly in the latter reaction and not at all in the (α, ^{3}He) are weak fragments of strength from a lower l rather than states populated by $i_{\frac{13}{2}}$ or $j_{\frac{15}{2}}$ transfer. Similarly level 23 at 1522 keV appears to contain a mixture of low- and high-l strength, the latter being selectively studied in the (α, ^{3}He) reaction. In addition, two new levels at about 2072 and 2110 keV appear in the (α, ^{3}He) spectrum but are buried in the $d_{\frac{5}{2}}$ strength in the (d, p) reaction. These levels have been assigned $l = 7$ ($j_{\frac{15}{2}}$) transfers because of their large strength in the (α, ^{3}He) reaction and because their energies are probably too high for them to be part of the $\pi h_{\frac{9}{2}} \nu i_{\frac{13}{2}}$ multiplet.

Many of the levels populated by $i_{\frac{13}{2}}$ or $j_{\frac{15}{2}}$ neutron transfer have only been observed in neutron transfer reactions, and no independent spin determinations have been made for them. Thus we can determine whether the present data can be interpreted in a manner consistent with a weak-coupling structure, but a critical test of the model would require independent spin measurements for the states involved.

Suggested spin assignments based on the present data are given in table 4. In some cases, strengths of $l = 7$ states appear to be somewhat higher in the (d, p) than in the (α, ^{3}He) measurements. This reflects the problems of observing these weak transitions in the presence of possible background from weak, low-l transitions which may appear with comparable cross section in the (d, p) reaction. An identification of all expected states can be suggested, with only the 11^+ state of the $\pi h_{\frac{9}{2}} \nu j_{\frac{15}{2}}$ multiplet fragmented. The decision to assign the level at 2110 as a fragment of the 11^+ rather than the 8^+ strength was made largely on the basis of Kuo and Herling's calcula-

tions [13]) which predict that the 11^+ member of the $\pi h_{\frac{9}{2}} \nu j_{\frac{15}{2}}$ multiplet should be above the 8^+ member.

4.3. THE $d_{\frac{5}{2}}$ AND $s_{\frac{1}{2}}$ NEUTRON TRANSFERS

In the present work there are ten levels which appear to be populated predominantly by a $d_{\frac{5}{2}}$ neutron transfer while in the simplest weak-coupling model the $\pi h_{\frac{9}{2}} \nu d_{\frac{5}{2}}$ multiplet should have its strength concentrated in only 6 states. The observed fragmentation is believed to result from the mixing of the $\pi h_{\frac{9}{2}} \nu d_{\frac{5}{2}}$ multiplet levels with members of the $\pi f_{\frac{7}{2}} \nu i_{\frac{13}{2}}$ configuration. In addition, a mixed-l analysis indicates some mixing of the $\pi h_{\frac{9}{2}} \nu d_{\frac{5}{2}}$ and $\pi h_{\frac{9}{2}} \nu s_{\frac{1}{2}}$ levels.

Sample angular distributions for these two multiplets are shown in figs. 8 and 9. The predominantly $d_{\frac{5}{2}}$ angular distributions for the levels at 2076, 2103 and 2173 keV show an unexpectedly large cross section between 40° and 50°. For the first two levels this is probably due to the $j_{\frac{15}{2}}$ transfers to levels at $\approx$ 2072 and $\approx$ 2110 keV. However, no such level occurs near 2173 keV. The analyses for these three levels to determine mixed $l = 0$ and $l = 2$ strengths are subject to fairly large uncertainties because an $l = 7$ standard was not simultaneously included in the analysis. For example, the analysis for the level at 2103 keV indicated a substantial mixture of $s_{\frac{1}{2}}$ strength. This interpretation was discarded because the allowed spins for the level would not permit such mixing. The uncertainties in the spectroscopic strengths for all levels indicated to be populated with mixed l-values have been obtained from the chi-squared distributions for the fits and are shown in table 4. The assigned spin values for all the levels are also shown. Because of the large amount of mixing and fragmentation seen for the $\pi h_{\frac{9}{2}} \nu d_{\frac{5}{2}}$ and $\pi h_{\frac{9}{2}} \nu s_{\frac{1}{2}}$ multiplets, these spin assignments should be regarded as tentative except where they are uniquely determined from the γ-decay of the level.

4.4. THE $g_{\frac{7}{2}}$ AND $d_{\frac{3}{2}}$ NEUTRON TRANSFER

The levels from $\pi h_{\frac{9}{2}} \nu g_{\frac{7}{2}}$ and $\pi h_{\frac{9}{2}} \nu d_{\frac{3}{2}}$ multiplets in ^{210}Bi are predicted to be fairly strongly mixed, and an analysis of the angular distributions for transitions populating levels in these configurations has revealed the presence of mixing. The results of this analysis are given in table 4. The mixing ratios were found to be strongly dependent on the exact shape of the standard curves, and an attempt was made to redo the analysis using DWBA curves. The results obtained were totally unrealistic, thus pointing up the importance of using the ^{208}Pb(d, p) curves as standards in the analysis.

Sample angular distributions for both mixed and pure transitions are shown in figs. 10–12. In general, the fits to the angular distributions are fairly good for states populated by mixed $g_{\frac{7}{2}}$ and $d_{\frac{3}{2}}$ neutron transfer, but the sensitivity of the data to changes in the mixing ratios is not as large as had been hoped, and a certain amount of judgement had to be exercised in interpreting the results. In cases where the chi-squared distributions were fairly flat and an uncertainty of one standard deviation

included a pure-l fit, the transitions were generally assigned as involving only the single-l transfer, while for most other cases, the minimum chi-squared mixing ratio was used. However, this procedure was not followed for three of the levels. Level 46 at 2729 keV was indicated to be significantly mixed, while the allowed spin values are not consistent with its containing any $d_{\frac{3}{2}}$ strength. It was therefore assumed to be populated by pure $g_{\frac{7}{2}}$ transfer. Levels 56 and 57 at 3136 and 3177 keV, respectively, were indicated to be mixed and primarily $g_{\frac{7}{2}}$, but their fits yield two of the three largest chi-square values found in this work and for each of them it was necessary to assume a predominance of $d_{\frac{3}{2}}$ strength to get a spectroscopic factor consistent with their allowed spin values. They have each been listed as pure $d_{\frac{3}{2}}$ in table 4.

4.5. TOTAL MULTIPLET STRENGTHS

The spectroscopic strengths for all levels assigned to a given multiplet have been added together to obtain a total strength for transferring a neutron into the corresponding single-particle level. For the $l = 0$, 2 and 4 neutron transfers, the experimental strengths for ^{210}Bi are based on the measured ^{208}Pb(d, p) angular distributions. The final numbers obtained thus give a measure of the strength observed in ^{210}Bi relative to the amount seen in ^{209}Pb. To the extent that the states in ^{209}Pb may be viewed as pure single-particle states, the present results may then be interpreted as indicating the validity of a simple two-particle model for describing the observed states of ^{210}Bi.

TABLE 5

Comparison of summed spectroscopic strengths in ^{210}Bi multiplets with the predicted strengths

Configuration	G_{exp}	G_{pp}
$\pi h_{\frac{9}{2}} \nu g_{\frac{7}{2}}$	10.6	10
$\pi h_{\frac{9}{2}} \nu i_{\frac{13}{2}}$	13.9 [a])	12
$\pi h_{\frac{9}{2}} \nu j_{\frac{15}{2}}$	18.6 [a])	16
$\pi h_{\frac{9}{2}} \nu d_{\frac{3}{2}}$	5.7	6
$\pi h_{\frac{9}{2}} \nu s_{\frac{1}{2}}$	2.1	2
$\pi h_{\frac{9}{2}} \nu g_{\frac{7}{2}}$	8.2	8
$\pi h_{\frac{9}{2}} \nu d_{\frac{3}{2}}$	3.8	4

[a]) Based on (α, ^{3}He) data with the assumed full strengths for the 10^- ($\pi h_{\frac{9}{2}} \nu i_{\frac{13}{2}}$) and 3^+ ($\pi h_{\frac{9}{2}} \nu j_{\frac{15}{2}}$) levels.

For the $\pi h_{\frac{9}{2}} \nu i_{\frac{13}{2}}$ and $\pi h_{\frac{9}{2}} \nu j_{\frac{15}{2}}$ multiplets, the total strengths have been estimated from the (α, ^{3}He) data assuming the full predicted strengths for the 3^+ and 10^- levels. These strengths are roughly consistent with the present (d, p) results. In addition, because of the poor resolution in the (α, ^{3}He) data the 1^- level populated in the $i_{\frac{13}{2}}$ transfer was not seen in this reaction. It has been tentatively identified from the present (d, p) work and its strength has been included in the sum.

The total spectroscopic strengths for the seven observed multiplets are summarized in table 5. Also shown are the expected values assuming that the states observed in ^{209}Pb are single-particle states. The agreement between the observed and predicted strengths is, in most cases, remarkably good, better than that for the individual spin

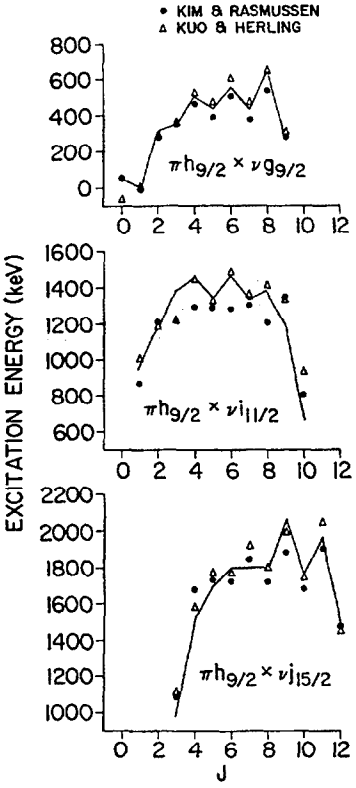

Fig. 13. Structure of the $\pi h_{\frac{9}{2}} \nu g_{\frac{9}{2}}$, $\pi h_{\frac{9}{2}} \nu i_{\frac{11}{2}}$ and $\pi h_{\frac{9}{2}} \nu j_{\frac{15}{2}}$ multiplets. The lines connect the experimental centroid energies for neighboring spin values. The circles and triangles show the predicted energies of Kim and Rasmussen [11]) and of Kuo and Herling [13]) respectively.

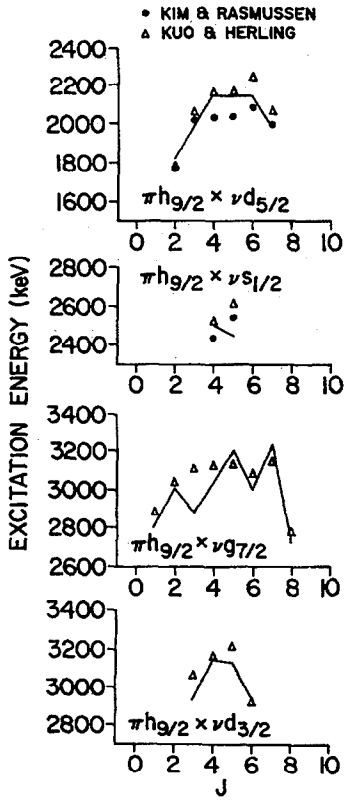

Fig. 14. Structure of the $\pi h_{\frac{9}{2}} \nu d_{\frac{5}{2}}$, $\pi h_{\frac{9}{2}} \nu s_{\frac{1}{2}}$, $\pi h_{\frac{9}{2}} \nu g_{\frac{7}{2}}$ and $\pi h_{\frac{9}{2}} \nu d_{\frac{3}{2}}$ multiplets. The points and lines have the same significance as in fig. 13.

members of the multiplets, particularly the $\pi h_{\frac{9}{2}} \nu g_{\frac{7}{2}}$ and $\pi h_{\frac{9}{2}} \nu d_{\frac{3}{2}}$ configurations. The greatest deviations are for the $i_{\frac{11}{2}}$ and $j_{\frac{15}{2}}$ neutron transfer where the experimental strengths are about 15 % high. This may be because the DWBA calculations overestimate the Q-dependence of the cross section. The results of table 5 indicate that all the single-particle strength has been found.

5. Comparison with model calculations

5.1. MULTIPLET STRUCTURE

The structure of the observed multiplets is conveniently displayed by plotting the energy of each member of the multiplet versus spin as shown in figs. 13 and 14. For levels exhibiting configuration mixing, the energy shown is the centroid of the observed components. Also shown in these figures are the centroid energies as calculated by Kuo and Herling [13]) and by Kim and Rasmussen [11]).

The comparisons in figs. 13 and 14 indicate that either calculation can account for the general trends of the data; in particular, the relatively low energies of the states of highest and lowest spins for a given configuration. On the other hand, neither calculation can account for all the details in the data. For the ground state multiplet, both sets of theoretical numbers agree quite well with the data, but the Kuo and Herling calculations achieve this agreement without adjusting any parameters. They also do about equally well in predicting the $\pi h_{\frac{9}{2}} \nu j_{15/2}$ and $\pi h_{\frac{9}{2}} \nu s_{\frac{1}{2}}$ energies (the latter being somewhat uncertain experimentally because of configuration mixing). On the $\pi h_{\frac{9}{2}} \nu i_{13/2}$ and $\pi h_{\frac{9}{2}} \nu d_{\frac{5}{2}}$ multiplets, the Kuo and Herling results seem to be slightly better. In fact, the overall agreement between the data and the Kuo-Herling calculations is quite impressive.

5.2. CONFIGURATION MIXING

The experimental results for ^{210}Bi show much more evidence of configuration mixing than was found for the ^{208}Bi nucleus [19]) or for the ^{210}Po nucleus [20]). This is presumably because the neutron-particle levels are more closely spaced than the proton-particle and neutron-hole levels. In general, theoretical calculations also produce more mixing for ^{210}Bi, the most complete calculations which include a tensor force component being those of Kuo and Herling [13]).

For the ground state multiplet, the Kuo and Herling calculations predict that all the levels should be better than 96 % pure, while experimentally only the 8^- level shows significant fragmentation. This fragmentation was first reported in some preliminary results of this work [21]) and was later confirmed by Kolata and Daehnick [16]). It is presumably due to mixing with the 8^- level of the $\pi f_{\frac{7}{2}} \nu g_{\frac{9}{2}}$ multiplet. This level is predicted to be one of the lowest in energy in its configuration while the $\pi h_{\frac{9}{2}} \nu g_{\frac{9}{2}}$ 8^- level lies fairly high in its multiplet.

For the $\pi h_{\frac{9}{2}} \nu i_{13/2}$ multiplet, no fragmentation of strength was observed. Kuo and Herling predict significant mixing with the $\pi f_{\frac{7}{2}} \nu g_{\frac{9}{2}}$ configuration for spins of 1^-, 2^-, 3^- and (to a lesser extent) 5^-.

For the $\pi h_{\frac{9}{2}} \nu j_{15/2}$ multiplet, the only predicted mixing is for the 9^+ level. While the data are not definitive in this regard, the present indication is for mixing of the 11^+ rather than the 9^+ member of the multiplet.

The $\pi h_{\frac{9}{2}} \nu d_{\frac{5}{2}}$ multiplet is both predicted and found to be severely fragmented, primarily due to the proximity of the $\pi f_{\frac{7}{2}} \nu i_{13/2}$ multiplet. The $\pi h_{\frac{9}{2}} \nu d_{\frac{5}{2}}$ multiplet is also predicted and found to be mixed with the $\pi h_{\frac{9}{2}} \nu s_{\frac{1}{2}}$ configuration. The calculated and

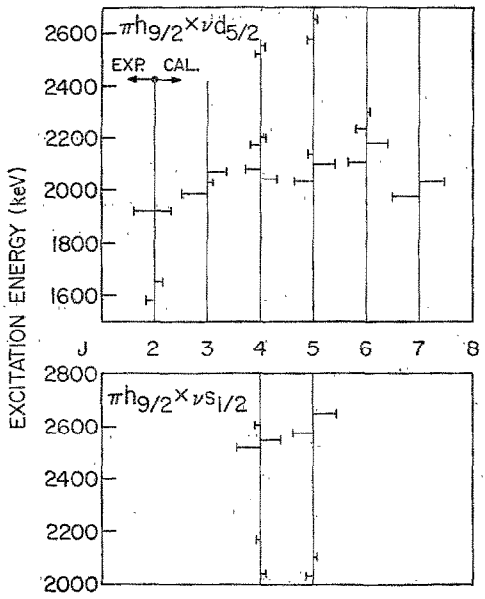

Fig. 15. Fragmentation of strength in the $\pi h_{\frac{9}{2}} \nu d_{\frac{5}{2}}$ and $\pi h_{\frac{9}{2}} \nu s_{\frac{1}{2}}$ multiplets. The calculated values are those of Kuo and Herling [13]). The lengths of the horizontal bars indicate the fraction of the total strength of that spin in the configuration which is observed or predicted to be at that energy.

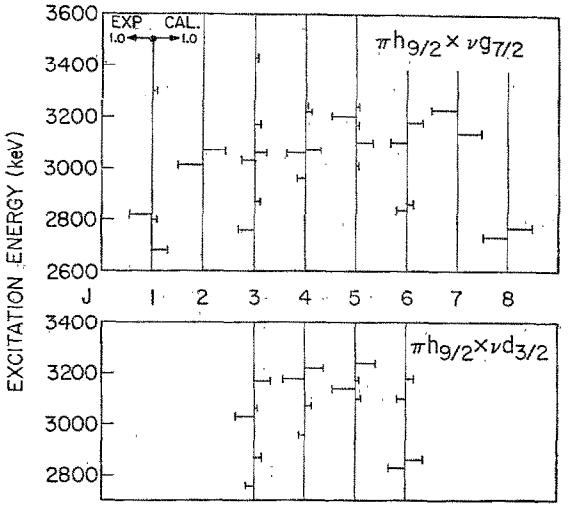

Fig. 16. Fragmentation of strength in the $\pi h_{\frac{9}{2}} \nu g_{\frac{7}{2}}$ and $\pi h_{\frac{9}{2}} \nu d_{\frac{3}{2}}$ multiplets. All symbols have the same significance as in fig. 15.

experimental (d, p) strengths for $d_{\frac{5}{2}}$ and $s_{\frac{1}{2}}$ neutron transfer are shown in fig. 15. The calculations are due to Kuo and Herling. The overall agreement is remarkably good for both multiplets except for the 3^- level in the $d_{\frac{5}{2}}$ neutron transfer for which no fragmentation is observed.

A similar comparison for the $g_{\frac{7}{2}}$ and $d_{\frac{3}{2}}$ neutron transfers is shown in fig. 16. Here the agreement between the calculated and observed amounts of configuration mixing is not quite as good as that seen in fig. 15. However, it is still quite satisfactory, especially considering the large uncertainties in the experimental mixing ratios (see table 4).

In general then, with the exception of the $\pi h_{\frac{9}{2}} \nu i_{\frac{13}{2}}$ multiplet, the calculations of Kuo and Herling predict amounts of configuration mixing which are in good agreement with our experimental results. It should be kept in mind here that while some of the spin assignments made in this work have been influenced by predicted level orderings, the experimental mixing ratios and fragmentations are generally independent of all theoretical calculations.

6. Conclusions

In the present work, we have observed the two-particle multiplets in ^{210}Bi arising from the coupling of an $h_{\frac{9}{2}}$ proton with a neutron in one of the orbits of the lowest unfilled oscillator shell. The combination of (d, p) and (α, ^{3}He) results has provided much new information on states of the $i_{\frac{13}{2}}$ and $j_{\frac{15}{2}}$ multiplets while the use of ^{208}Pb(d, p) angular distributions as standard curves has simplified the interpretation of the ^{209}Bi(d, p) data.

The present results indicate that all the strength of the seven neutron single-particle states in ^{209}Pb has been located in the multiplets of ^{210}Bi. The distribution of strength within each multiplet is generally consistent with a simple two-particle weak-coupling model for the structure of the observed multiplets, though some configuration mixing is seen.

The multiplet structures are very well reproduced by the calculations of Kuo and Herling [13]) and are also fitted fairly well by earlier calculations of Kim and Rasmussen [11]). It may be noted that both these calculations assume tensor forces in the effective interaction. A recent RPA calculation of Vary and Ginocchio [12]) which has no tensor force contributions is, as anticipated by those authors, notably less successful in fitting the data, while similar calculations on neighboring nuclei have done very well in accounting for experimental results.

In a more detailed comparison, the calculations of Kuo and Herling [13]) are reasonably successful in predicting the observed fragmentations of the multiplets with an $h_{\frac{9}{2}}$ proton coupled to neutrons in the $d_{\frac{5}{2}}$ and $s_{\frac{1}{2}}$ or $g_{\frac{7}{2}}$ and $d_{\frac{3}{2}}$ orbitals. They also predict the almost complete lack of fragmentation for the $\pi h_{\frac{9}{2}} \nu g_{\frac{9}{2}}$ and $\pi h_{\frac{9}{2}} \nu j_{\frac{15}{2}}$ multiplets. Only the splitting of the 8^- member of the ground state configuration and the 11^+ member of the $\pi h_{\frac{9}{2}} \nu j_{\frac{15}{2}}$ multiplet is not predicted. Kuo and Herling predict significant mixing of the 1^-, 2^- and 3^- members of the $\pi h_{\frac{9}{2}} \nu i_{\frac{13}{2}}$ multiplet with the $\pi f_{\frac{7}{2}} \nu g_{\frac{9}{2}}$ configuration which is not populated by neutron transfer reactions. While no such fragmentation of the $i_{\frac{13}{2}}$ strength is observed, these states are quite weak, and the data are far from definitive.

References

1) B. H. Wildenthal, B. M. Preedom, E. Newman and M. R. Cates, Phys. Rev. Lett. **19** (1967) 960
2) J. Bardwick and R. Tickle, Phys. Rev. **171** (1968) 1305
3) P. Mukherjee and B. L. Cohen, Phys. Rev. **127** (1963) 1284
4) G. Muehllehner, A. S. Poltorak, W. S. Parkinson and R. H. Bassel, Phys. Rev. **159** (1967) 1039
5) G. J. Igo, P. D. Barnes, E. R. Flynn and D. D. Armstrong, Phys. Rev. **177** (1969) 1831
6) J. R. Erskine, W. W. Buechner, H. A. Enge, Phys. Rev. **128** (1962) 720
7) P. Mukherjee, Phys. Rev. **131** (1963) 2162
8) R. Ley, Diplomarbeit, Max-Planck-Institut für Kernphysik, Heidelberg, 1970, unpublished
9) C. Ellegaard, P. D. Barnes, R. Eisenstein and T. R. Canada, Phys. Lett. **35B** (1971) 145
10) H. T. Motz, E. T. Jurney, E. B. Shera and R. K. Sheline, Phys. Rev. Lett. **26** (1971) 854
11) Y. E. Kim and J. O. Rasmussen, Nucl. Phys. **47** (1963) 184
12) J. Vary, Ph.D. thesis, Yale University, 1970, unpublished;
J. Vary and J. N. Ginocchio, Nucl. Phys. **A166** (1971) 479 and J. N. Ginocchio, private communication
13) T. T. S. Kuo and G. H. Herling, Naval Research Laboratory NRL memorandum report 2258 (1971)
14) P. D. Kunz, The program DWUCK, University of Colorado, unpublished
15) S. A. A. Zaidi and S. Darmodjo, Phys. Rev. Lett. **19** (1957) 1446
16) J. J. Kolata and W. W. Daehnick, Bull. Am. Phys. Soc. **16** (1971) 623 and University of Pittsburgh preprint
17) J. S. Boyno, Th. W. Elze and J. R. Huizenga, Nucl. Phys. **A157** (1970) 263
18) W. P. Alford and D. G. Burke, Phys. Rev. **185** (1969) 1560
19) W. P. Alford, J. P. Schiffer and J. J. Schwartz, Phys. Rev. **C3** (1971) 860
20) W. A. Lanford, W. P. Alford and H. W. Fulbright, University of Rochester NSRL-44
21) C. K. Cline, W. P. Alford and H. E. Gove, Bull. Am. Phys. Soc. **16** (1971) 79
22) J. R. Erskine and W. H. Buechner, Bull. Am. Phys. Soc. **7** (1962) 360